

## Mechanical properties optimization and microstructures of diffusion bonded AA2014/AA7075 al alloys

Antony Sagai Francis Britto<sup>a</sup>, Joseph Selvi Binoj<sup>b,\*</sup>

<sup>a</sup> Department of Mechanical Engineering, Rohini College of Engineering & Technology, Palkulam- 629401, Tamil Nadu, India

<sup>b</sup> Institute of Mechanical Engineering, Saveetha School of Engineering, Saveetha Institute of Medical and Technical Sciences (SIMATS), Chennai- 602105, Tamilnadu, India

(\*Corresponding author: [binojlaxman@gmail.com](mailto:binojlaxman@gmail.com))

Submitted: 13 November 2021; Accepted: 10 October 2022; Available On-line: 08 November 2022

**ABSTRACT:** Diffusion bonding has been successfully used to join dissimilar high-strength aluminium alloys. In bonding AA2014 with AA7075 aluminium alloy, the main diffusion bonding process parameters were optimized to achieve optimum shear and ram tensile strengths. For the strategical planning of experiments, the design of experiment concept was used, as well as the response surface methodology to create statistical models for optimizing the process parameters. The bond strength improved as the interface thickness increased, but above 6  $\mu\text{m}$  (at about 375 °C), the bond strength began to deteriorate. Similarly, the stiffness of the joint interface increased as the process temperature increased due to the development of interfacial phases. The empirical findings were evaluated, and the optimal bonding range was determined in order to maximize the bond's shear and ram tensile strength.

**KEYWORDS:** Aluminium alloy; Diffusion bonding; Mechanical properties; Microstructural characterization; Optimization

Citation/Citar como: Britto, A.S.F.; Binoj, J.S. (2022). "Mechanical properties optimization and microstructures of diffusion bonded AA2014/AA7075 al alloys". *Rev. Metal.* 58(3): e225. <https://doi.org/10.3989/revmetalm.225>

**RESUMEN:** *Optimización de las propiedades mecánicas y microestructuras de las aleaciones de aluminio AA2014/AA7075 unidas por difusión.* La unión por difusión se ha utilizado con éxito para unir diferentes aleaciones de aluminio de alta resistencia. Al unir las aleaciones de aluminio AA2014 y AA7075, se optimizaron los principales parámetros del proceso para lograr resistencias óptimas por cizallamiento y bajo ensayo ram de tracción. Para la planificación estratégica de los experimentos se utilizó el concepto de diseño de experimentos, así como la metodología de superficie de respuesta para crear modelos estadísticos que permitan optimizar los parámetros del proceso. La fuerza de unión mejoró a medida que aumentaba el grosor de la zona de unión, pero por encima de 6  $\mu\text{m}$  (a aproximadamente 375 °C), la fuerza de unión comenzó a deteriorarse. De manera similar, la rigidez de la interfaz de la junta aumentó a medida que aumentaba la temperatura del proceso debido al desarrollo de las fases en la intercara de unión. Se evaluaron los resultados empíricos y se determinó el rango de unión óptimo para maximizar la resistencia de la unión por cizallamiento y bajo ensayo ram de tracción.

**Copyright:** © 2022 CSIC. This is an open-access article distributed under the terms of the Creative Commons Attribution 4.0 International (CC BY 4.0) License.

**PALABRAS CLAVE:** Aleación de aluminio; Caracterización microestructural; Optimización; Propiedades mecánicas; Unión por difusión

**ORCID ID:** Antony Sagai Francis Britto (<https://orcid.org/0000-0002-5814-5240>); Joseph Selvi Binoj (<https://orcid.org/0000-0002-7222-4463>)

## 1. INTRODUCTION

The growing use of composite materials is likely to fill the role of pure aluminium in aircraft. High-strength aluminium alloys like AA2014 and AA7075, on the other hand, are still essential airframe materials. Even though the composite material percentages in fighter aircraft are only 40–50 percent, aluminium alloys play a significant role (Campbell, 2006). Their unique properties, such as high specific strength, superior malleability, ease of machining, excellent corrosion resistance, and strong thermal and electrical conductivity, are increasingly being used (Grard, 1920). Various welding methods are used to join them. The results of TIG welding techniques on 2219 aluminium welded joints were investigated (Li *et al.*, 2017). Plasma-MIG hybrid welding was used to join Al 5083 aluminium alloys (Cai *et al.*, 2018). The disc laser beam welding technique was used to join 2A14-T6 aluminium alloys (Wang *et al.*, 2018). Fiber laser-GMAW hybrid welding techniques were used to join Al 5083 aluminium alloys (Huang *et al.*, 2018). However, due to the formation of oxide films and the lack of matching filler metals with identical solidification modes, traditional methods of joining them are ineffective (Ilangoan *et al.*, 2015). Solid state diffusion bonding, on the other hand, prevents crack formation, significant distortion, and grain boundary segregation in the base metal (Wu and Lo, 2002; Zhao and Zhang, 2008; Wang *et al.*, 2012; Britto *et al.*, 2020). Bonding temperature, bonding strength, and holding time are the most important parameters in diffusion bonding, with temperatures held at 0.5 to 0.8 times the melting point of the parent metal with the lowest melting point (Hill and Wallach, 1989; He *et al.*, 2002; Mahendran *et al.*, 2009). The bonding pressures should be high enough to fill interfacial voids and disperse surface oxide films (Kazakov, 1985). In general, the holding time is held to a bare minimum to ensure that a proper metallic bond is formed across the interface without forming an excessively thick inter-diffusion/reaction layer (Peterson *et al.*, 2004; Palanisamy *et al.*, 2021).

In both air and nitrogen atmospheres, solid-state diffusion bonding of an aluminium silicon cast alloy (Al-390) was investigated. To avoid oxidation of the faying surfaces, the samples were silver coated. The tensile strength of the bonds formed in a nitrogen atmosphere was good, about 57 MPa, while the bonds formed in an atmosphere had virtually no strength (Morley and Caruso, 1980). By chemically treating Al-7475 alloys in NaOH and HNO<sub>3</sub>, an attempt was made to use solid-state diffusion bond-

ing. Bonding in atmospheric conditions yielded shear strengths in the range of 30-150 MPa (Pilling and Ridley, 1987). Diffusion bonding with aluminium alloy 7475 at superplastic temperatures resulted in more cavities in the joints (Sunwoo and Lum, 1995). Pre-treatment of the surface of the AA8090 aluminium alloy resulted in a narrow bond line, similar to that of a grain boundary, with high bond strength (Wu and Lo, 2002). In superplastic 7075 aluminium alloy, the effect of diffusion bonding parameters such as temperature, strain, and time on specific strength was investigated, and it was discovered that proper bonding did not occur until 500 °C at nominal pressures. The effect of bonding pressure increases as the pressure rises above 3.8 MPa. The following is a list of the ideal conditions for successful bonding: Temperature of 510-520 °C, pressure of 2.5-3.8 MPa, and time of keeping 90-120 min (Huang *et al.*, 1999). Diffusion bonding was used to join aluminium alloys 8090 and 7475, and similar results were published (Sunwoo, 1993). Response surface methodology (RSM) was used to optimise process parameters, and it was found to be successful in dealing with possible interaction effects among variables (Huiping *et al.*, 2007). RSM dealt with multi-variable process dynamics and developed a stable model with fewer trials (Velmanirajan *et al.*, 2012).

Diffusion bonding literature is scarce and insufficient to develop this technique, necessitating further research in solid-state processes to join dissimilar Al alloys for a variety of engineering applications. Diffusion bonding of AA2014 and AA7075 Al alloys was investigated in this study in order to optimize the major influencing process parameters, such as bonding temperature, strain, and holding time, in order to maximize bond power. For the first time, microstructural findings were corroborated with mechanical properties such as shear and ram tensile strength to define and optimize process conditions using a multi-variant method.

## 2. MATERIALS AND METHODS

### 2.1. Experimental procedure and design

For the diffusion bonding sample, a 6 mm thick aluminium alloy in grades AA2014 and AA7075 was obtained from M/s. PMC corporation in Bangalore, India and machined to a scale of 50x50 mm. Table 1 shows the chemical composition of the Al alloys that were examined. The specimen's surfaces were polished with SiC paper of 200#, 400#, and 600#

TABLE 1. Chemical composition of the base materials in wt. %

	Al	Zn	Mn	Fe	Ti	Si	Cu	Cr	Mg
AA 2014	93.15	0.25	0.60	0.70	-	0.80	4.00	0.10	0.40
AA7075	90.02	5.10	0.30	0.50	0.20	0.40	1.20	0.18	2.10

grit and then cleaned with acetone before being subjected to diffusion bonding (Britto *et al.*, 2017; Britto *et al.*, 2022).

Figure 1 depicts the diffusion bonding setup (a). The specimens were placed into a special 316L stainless steel die assembly (Fig. 1b) and interleaved into a vacuum chamber (see Fig. 1c) maintained at 29 mm Hg (Fernandus *et al.*, 2012) to minimize oxidation. With the aid of a PID controller, the temperature of the specimen can be raised at a rate of  $25\text{ }^{\circ}\text{C}\cdot\text{min}^{-1}$  and maintained at the desired temperature. The hydraulic system, which is equipped with a load cell, is used to apply and calculate the necessary pressure. The specimen was cooled to room temperature for further characterization and testing after being held at the planned conditions for a specified period of time.



FIGURE 1. Experimental Setup, (a) Diffusion bonding machine; (b) 316L Stainless steel die; (c) Vacuum furnace.

## 2.2. Microstructural characterization

To reveal the microstructure, the specimen was polished with progressive grade SiC Paper and then etched with Keller's solution (190 ml distilled water, 5 ml nitric acid, 3 ml hydrochloric acid, and 2 ml hydrofluoric acid) (Kong *et al.*, 2004). An optical microscope (Make: MEIJI, Japan; Model: MIL-7100) was used to examine the microstructure of the interface bond, accompanied by a metallurgical microscope (Make: HUVITZ, Korea; Model: HRM-300M) to measure the thickness of the interface bond using 'panasis' software. Under a scanning electron microscope, energy-dispersive X-ray

spectroscopy (EDS) was used to map the elemental composition of micro-zones near the joints (Make: ZEISS, Germany; Model: EVO -18). X-ray diffraction (XRD) of CuK radiation, with a  $2\theta$  total range from  $0^{\circ}$  to  $80^{\circ}$  with a step size of  $0.02^{\circ}$  was performed to identify the phases present in the microstructure (Make: PANalytical; Model: X'Pert PRO). To make the indentation and calculate the diffusion layer hardness across the joint, Vickers used a 0.5 kg load and a dwell time of 10 sec on a microhardness tester (Make: SHIMADZU, Japan; Model: HMV-T1) (normal to the interface region).

## 2.3. Mechanical characterization

The lap shear and ram tensile strength of the bonds were determined using nonstandard test specimens. Figure 2 depicts the dimensional details of specimens. The lap shear specimens were machined with a spark erosion machine (Make: ELECTROICA, Japan; model: super cut-734) at a cutting speed of  $1.5\text{ mm}\cdot\text{min}^{-1}$ , while the ram tensile specimens were machined with an electric spark line cutting machine (Model: super cut-734) at a cutting speed of  $1.5\text{ mm}\cdot\text{min}^{-1}$  (Make: ELEKTRA, Japan; model: cut-500). Both tests were performed at a constant ram speed of  $5\text{ mm}\cdot\text{min}^{-1}$  in a 100 kN capacity servo operated universal testing machine (Make: FIE-BLUESTAR, India; Model UNITEK 94100) with data acquisition system. Figure 2 depicts the lap shear and ram tensile test specimens.

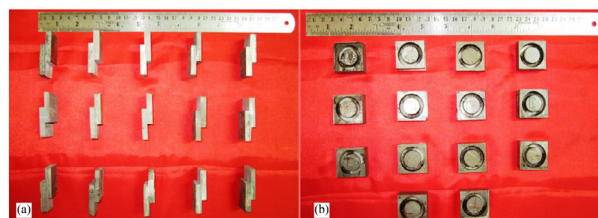
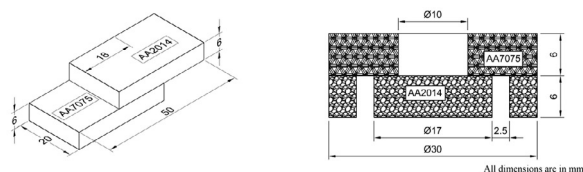


FIGURE 2. Dimension and photographic view of diffusion bonded samples for: (a) Lap Shear, and (b) Ram Tensile tests.

A three-factor, five-level central composite design (CCD) was chosen for testing in this research. Twen-

ty joints were created using the designed combinations of bonding process parameters such as temperature, bonding pressure, and holding time based on the design matrix. Due to insufficient thermal excitation to cause atom diffusion, good bonding was not achieved until 325 °C, and temperatures above 425 °C seem to be too high for sound bonding. Similarly, a bonding pressure of less than 2 MPa was insufficient to create enough contact points (between surface asperities) for atom diffusion to cross over. When the pressure is greater than 18 MPa, the specimens deform plastically, causing the outer edges to bulge. It has been discovered that diffusion requires

a minimum holding time of 15 min, and that holding times of more than 75 minutes are detrimental. The defined process parameters and their range are tabulated in Table 2 after several trial runs to examine the effect of the process parameters.

### 3. RESULTS AND DISCUSSION

Table 3 lists the shear and ram tensile strength of the specimens evaluated in triplicate of the bonded joints at various process parameters. After that, the data was analyzed using “response surface methodology (RSM)”.

TABLE 2. Feasible working limits of diffusion bonding parameters

S. N°	Parameter	Test Levels				
		(-α)	(-1)	(0)	(1)	(α)
1	Bonding temperature (T), °C	325	350	375	400	425
2	Bonding pressure (P), MPa	2	5	10	15	18
3	Holding time (H), min	15	30	45	60	75

TABLE 3. Shear and Ram Tensile strength of the bonded joints along with process parameter and diffusion layer thickness

Expt. N°	Temp, °C	Pressure, MPa	Holding Time, min	Shear Strength, MPa	Ram tensile Strength, MPa	Diffusion Layer Thickness, μm
1	350	5	30	40.1 ± 0.8	56.1 ± 1.4	1.72 ± 0.17
2	400	5	30	59.3 ± 2.3	72.1 ± 0.8	2.25 ± 0.08
3	350	15	30	37.3 ± 2.2	51.2 ± 2.6	0.93 ± 0.01
4	400	15	30	75.8 ± 2.1	88.8 ± 0.7	5.18 ± 0.09
5	350	5	60	36.1 ± 2.2	49.2 ± 1.2	0.85 ± 0.03
6	400	5	60	56.1 ± 0.7	68.5 ± 1.2	7.38 ± 0.18
7	350	15	60	33.7 ± 0.4	44.3 ± 0.3	0.67 ± 0.02
8	400	15	60	70.5 ± 0.8	84.9 ± 1.3	5.31 ± 0.15
9	325	10	45	23.4 ± 1.5	35.1 ± 0.5	0.35 ± 0.03
10	425	10	45	77.2 ± 0.8	89.8 ± 0.9	5.40 ± 0.32
11	375	2	45	41.1 ± 2.7	56.1 ± 1.1	1.42 ± 0.12
12	375	18	45	52.4 ± 1.8	68.0 ± 0.7	2.21 ± 0.06
13	375	10	15	48.1 ± 0.8	65.3 ± 1.0	1.62 ± 0.02
14	375	10	75	42.5 ± 1.9	57.76 ± 0.9	9.363 ± 0.05
15	375	10	45	82.2 ± 0.67	93.35 ± 0.5	3.872 ± 0.07
16	375	10	45	81.5 ± 0.6	91.76 ± 1.4	3.768 ± 0.06
17	375	10	45	83 ± 0.84	93.16 ± 1.7	3.854 ± 0.12
18	375	10	45	83.3 ± 1.5	93.12 ± 1.1	3.865 ± 0.14
19	375	10	45	83.5 ± 1.2	93.68 ± 0.9	3.798 ± 0.09
20	375	10	45	84.1 ± 0.7	93.78 ± 0.6	3.877 ± 0.10

### 3.1. Microstructural analysis

The thickness of the diffusion layer has a major impact on the diffusion bond's shear and tensile strength. Due to a lack of diffusion, a thin inter-diffusion area forms, resulting in a poor bond power. On the other

hand, excessive diffusion of materials causes deeper penetration at the inter-diffusion area of the elements resulting in a dense diffusion layer and poor bonding.

The microstructure of the different test samples, as well as their interface thickness, are shown in Fig. 3. The average interface thickness ranges



Figure. 3. Optical images of the microstructures of the joints showing the interface thickness variation for different bonding conditions.

from 0.346  $\mu\text{m}$  to 9.363  $\mu\text{m}$ , as determined by the programme for a specific specimen at different locations. Figure 4 depicts the relationship between the bond thickness and weight. The strength of the bond increases as the inter-diffusion element's area thickness increases up to 6  $\mu\text{m}$ , but as the interface thickness increases further, the bond strength decreases. This may be due to the presence of more inter-diffusion area of element constituents such as  $\text{Al}_3\text{Ti}_{0.75}\text{Fe}_{0.25}$ ,  $\text{Al}_2\text{MgCu}$ ,  $\text{Mg}_2\text{Si}$ , and  $\text{MgZn}_2$ , resulting in decreased material strength (Fig. 5). Also, the presence of transition metals such as Mg, Cu, Zn, Fe, and Ti in the bonding alloys is revealed by chemical examination, indicating that they form these inter-diffusion area during diffusion. The element mapping of the bonded surface was used to determine the degree of diffusion of a specific element from one material to the other (Fig. 6). The percentage content of a particular element in the parent metal before bonding, such as Mg, Cu, Zn, Si, Fe, and Ti, was noted above each elemental mapping micrograph (Fig. 6). These mapping micrographs will reveal the extent of each element's diffusion after the diffusion process.

For example, while AA2014 alloy does not contain Ti (Fig. 6f), it can be seen that Ti has diffused from AA7075 alloy to AA2014 alloy. Furthermore,

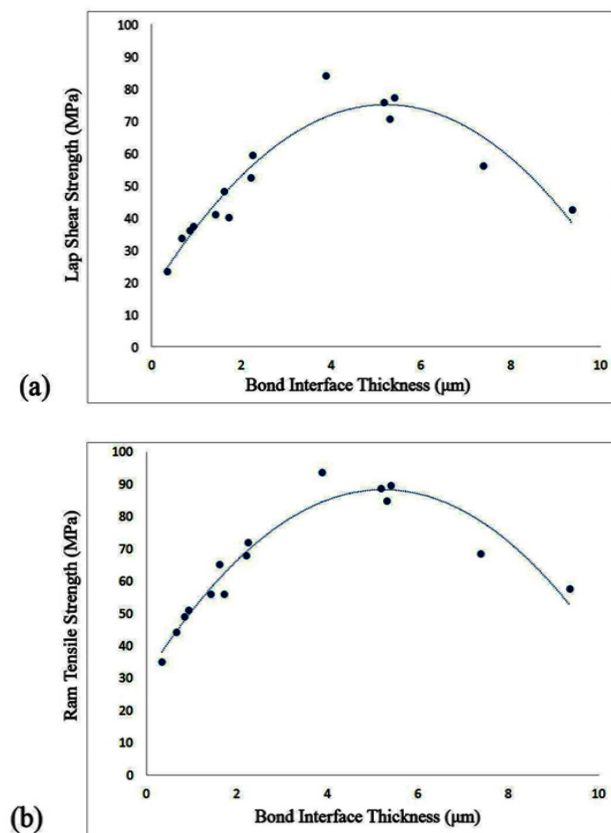


Figure 4. Correlation of bond interface thickness with that of (a) Lap Shear strength, and (b) Ram Tensile strength.

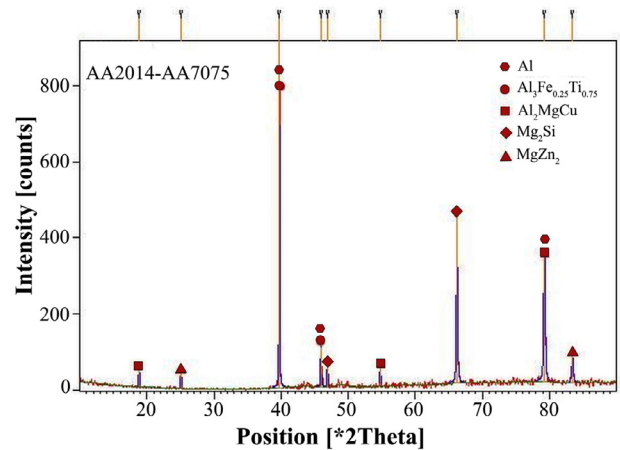


FIGURE 5. XRD pattern of diffusion bonded AA2014 and AA7075 aluminium plates. The experimental joining condition used are 375  $^{\circ}\text{C}$ , 45 min and 10 MPa.

X-ray diffraction analysis of the bonded joints confirmed the presence of inter-diffusion area of elements produced during diffusion (Fig. 5). To classify the phases, the X-ray diffraction patterns were analyzed and compared to Joint Committee on Powder Diffraction Standards (JCPDS) results. In addition, through the elemental mapping, it was confirmed that the reported peaks belong to  $\text{Al}_3\text{Ti}_{0.75}\text{Fe}_{0.25}$ ,  $\text{Al}_2\text{MgCu}$ ,  $\text{Mg}_2\text{Si}$ , and  $\text{MgZn}_2$ , as noted in the microstructural image.

The microhardness plot of some diffusion bonded joints was studied 5 mm away from the fusion line on both sides of the interface zone (Fig. 7). For the high strength bonds (Exp. No: 10, 20), a standard bell-shaped curve was obtained, with 190 Hv and 180 Hv reported in the interface area, respectively. The effect of diffusion can be seen up to 3 mm on either side of the joint due to differences in the parent metal's hardness. On the other hand, it was observed that maximum strength was not achieved either for more or less inter-diffusional areas (Fig. 3 and Fig. 4) due to the inability of the material to withstand the applied load. Hence, it should be emphasized that in diffusion bonding, an optimum narrow area such as 6  $\mu\text{m}$  formation at the inter-diffusion of elements is needed to achieve a higher bond strength.

### 3.2. Analysis of mechanical properties and process optimization

The interaction of process variables such as the bonding temperature, the pressing load, and the pressure application length is important, and a single adjustment at a time procedure is insufficient to draw successful control, necessitating a multi-variate method for experimentation and study. The significance and suitability of the established empirical models to relate the relationship of process param-

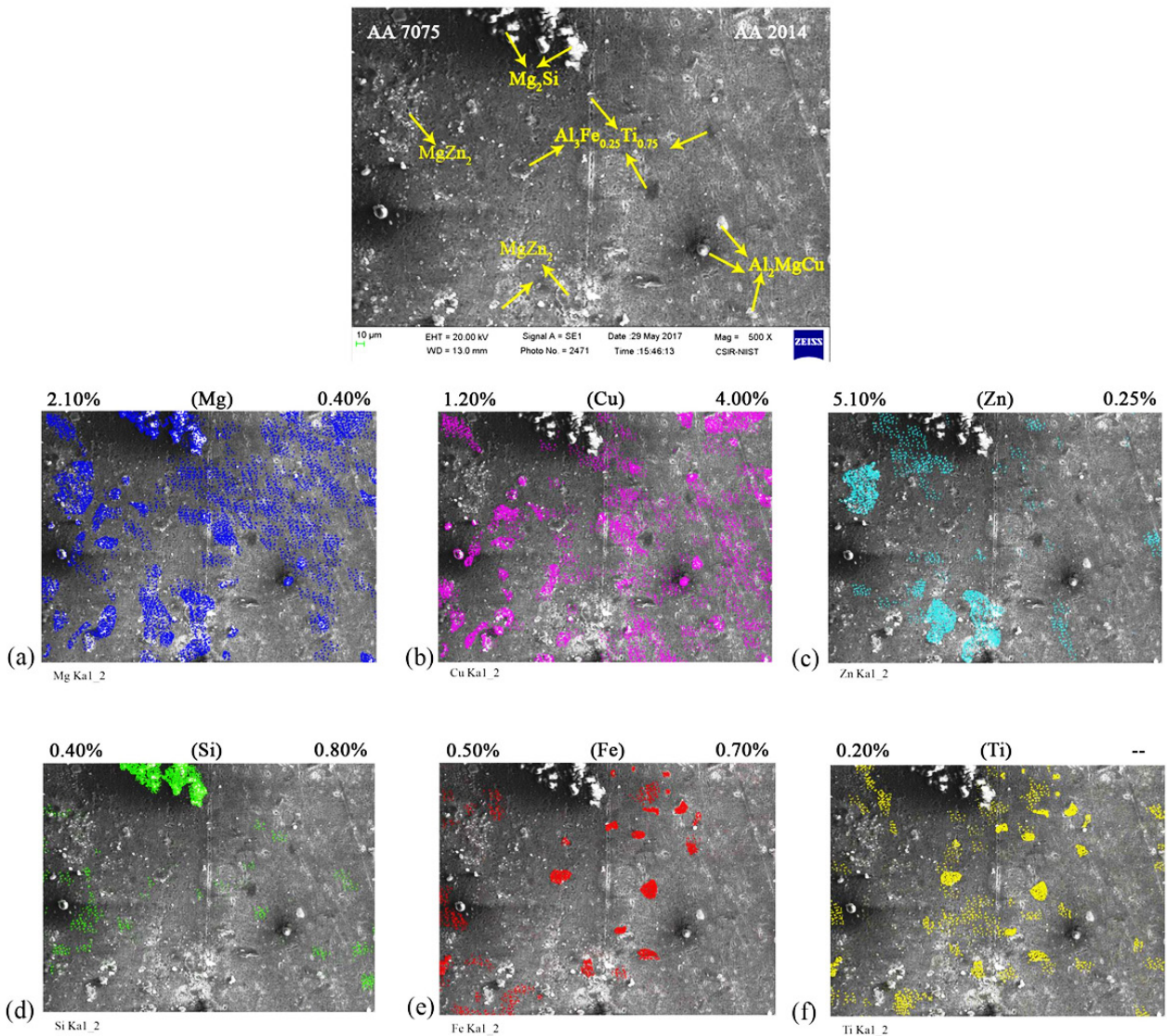


FIGURE 6. SEM images of the bonded microstructure obtained after joining two plates of AA2014 and AA7075 aluminium alloys. The corresponding elemental maps of the different chemical elements of the composition are shown in (a) Mg, (b) Cu, (c) Zn, (d) Si, (e) Fe, (f) Ti. The experimental joining condition used are 375 °C, 45 min and 10 MPa.

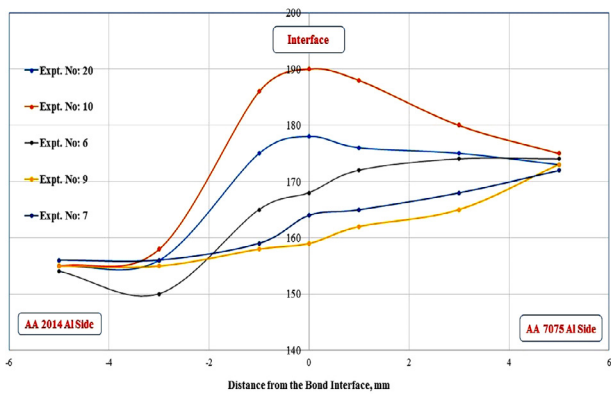


FIGURE 7. Vickers microhardness evolution along the interphase of the bonded joints normal to interface plane.

ters with the ram tensile and lap shear strength were confirmed using analysis of variance (ANOVA). Tables 4 and 5 show the ANOVA results for shear and ram tensile power, respectively.

Table 4 shows that the shear strength model's p-value is very tiny, indicating that the model is significant. The model's fitness is demonstrated by its  $R^2$  determination coefficient, which is 0.9988, implying that the overall variability is 99.88% when all the relevant variables are taken into account. The overall deviation outside of the model's preview is less than 1%. The 0.9933 expected R-Square value is in reasonable accordance with the 0.9977 Adjusted R-Squared value. The adequacy precision ratio is far higher than 4 at 85.365, indicating that the signal is adequate. The coefficient of variance, which cal-

TABLE 4. ANOVA results for the shear strength model

Source	Sum of Squares	df	Mean Square	F Value	p-value Prob > F	
Model	8194.9	9	910.6	907.3	< 0.0001	Significant
A	3082.2	1	3082.2	3071.2	< 0.0001	
B	145.3	1	145.3	144.7	< 0.0001	
C	46.6	1	46.6	46.4	< 0.0001	
AB	163.2	1	163.2	162.6	< 0.0001	
AC	0.07	1	0.09	0.09	0.8	
BC	0.3	1	0.3	0.3	0.6	
A <sup>2</sup>	1715.4	1	1715.4	1709.3	< 0.0001	
B <sup>2</sup>	2400.9	1	2400.9	2392.4	< 0.0001	
C <sup>2</sup>	2272.06	1	2272.06	2263.9	< 0.0001	
Residual	10.04	10	1.0			
Lack of Fit	5.5	5	1.1	1.2	0.4	not significant
Pure Error	4.5	5	0.9			
Cor Total	8205	19				

Std.Dev.=1.00; Mean=59.56; C.V.%=1.68; R<sup>2</sup>=0.9988; AdjR<sup>2</sup>=0.9977; Pred R<sup>2</sup>= 0.9933, Adeq Precision=85.365

culates residual variability, is just 1.68%, indicating that the tests are more precise and reliable. Inferences can be drawn with respect to the variables since the majority of the model parameters match well.

The ANOVA analysis of the ram tensile strength model (Table 5) reveals that the model's determination coefficient is R<sup>2</sup> 0.9983, implying that the model explains 99.83 percent of the overall uncertainty when all significant variables are taken into account. The Adjusted R-Squared value of 0.996 is very similar to the Predicted R-Squared value of 0.989. The adequacy

accuracy, which indicates the signal's adequacy by measuring the signal to noise ratio as 75.7. The model's F-value of 667.6 and p-value of 0.0001 indicate that it is important enough to draw conclusions.

For lap shear and ram tensile power, the standard likelihood plot versus residuals indicates a consistent closeness to the straight line (Fig. 8a and Fig. 8b), implying that the errors are distributed normally and confirming the model significance (Kadaganchi *et al.*, 2015).

The perturbation map depicts the influence of a factor in the design space when controlling other var-

TABLE 5. ANOVA results for the ram tensile strength model

Source	Sum of Squares	df	Mean Square	F Value	p-value Prob > F	
Model	7292.6	9	810.3	667.6	< 0.0001	Significant
A	3102.5	1	3102.5	2556.06	< 0.0001	
B	135.6	1	135.6	111.7	< 0.0001	
C	83.00	1	83.00	68.4	< 0.0001	
AB	228.6	1	228.6	188.3	< 0.0001	
AC	5.00	1	5.00	4.1	0.0700	
BC	0.0041	1	0.0041	0.0033	0.9551	
A <sup>2</sup>	1551.7	1	1551.7	1278.4	< 0.0001	
B <sup>2</sup>	1840.6	1	1840.6	1516.4	< 0.0001	
C <sup>2</sup>	1642.2	1	1642.3	1353.01	< 0.0001	
Residual	12.1	10	1.2			
Lack of Fit	9.5	5	1.90	3.6	0.0940	not significant
Pure Error	2.7	5	0.53			
Cor Total	7304.8	19				

Std.Dev.=1.10; Mean=72.30; C.V.%=1.52; R<sup>2</sup>=0.9983; AdjR<sup>2</sup>=0.9968; Pred R<sup>2</sup>= 0.9893; Adeq Precision=75.7

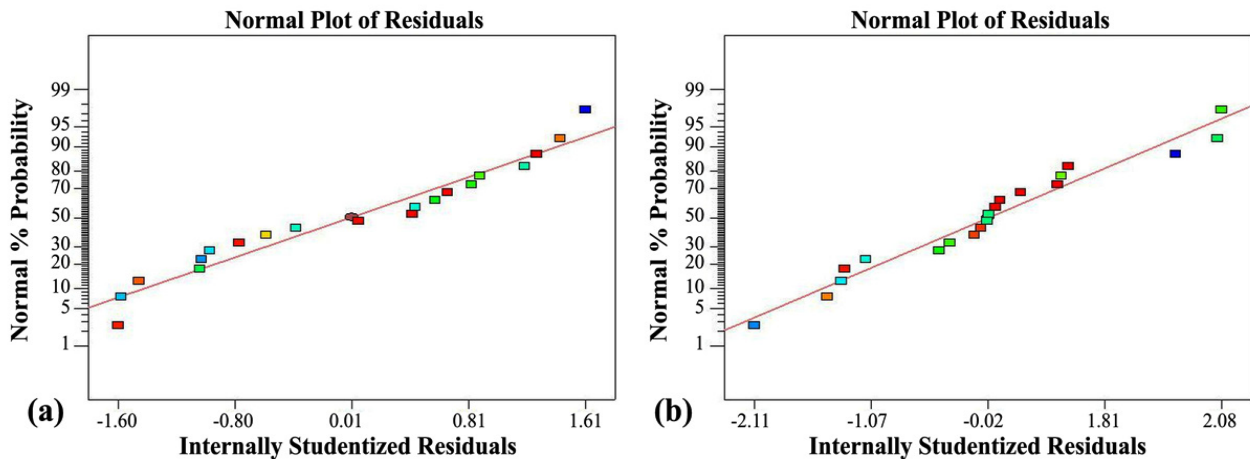


FIGURE 8. Normal probability plot of residuals for all experiment trials in different collurs: (a) Lap Shear and (b) Ram Tensile.

tables. The perturbation plot for the shear strength of diffusion bonded joints with respect to process variables including temperature, strain, and holding time is shown in Fig. 9a. The slope of the curve determines the influence of a factor. The temperature (factor A) is found to be the most influential factor in determining the bond's quality. The higher the applied temperature, the faster the atom Diffusion is. This diffusion is accompanied by a chemical reaction that creates a diffusion bond of a thickness wide enough to obtain an optimum strength in the joint. The shear strength rises with temperature up to about 400 °C, then falls as the temperature keeps increasing due to an excess in size of the inter-diffusion area as well as decohesion occurring between the materials. Similarly, pressure (factor

B) is a determining factor that must be maintained at around 10 MPa for proper bonding. Decreasing or rising the pressure has a negative impact on bond power, as does the holding time (factor C) of about 45 min.

Figure 9b shows the perturbation plots for Ram tensile strength, where (Factor A) is the most controlling parameter for the same purpose as shear strength. The effects of pressure (Factor B) and keeping time (Factor C) are close to those of shear strength, where it is best to maintain it at the experiment's mid-range value to have a better strength. The empirical results of bond strengths, lap shear power, and ram tensile with reference to the process parameters in the experimental context are used to construct statistical models, as shown below, Eq. (1) and Eq. (2).

$$\text{Shear Strength (MPa)} = -1978.62 + 10.02 \times A - 1.42 \times B + 3.78 \times C + 0.04 \times A \times B - 2.77E-004 \times A \times C - 2.68E-003 \times B \times C - 0.01 \times A^2 - 0.57 \times B^2 - 0.04 \times C^2 \quad (1)$$

$$\text{Ram Tensile Strength (MPa)} = -1791.31 + 9.37 \times A - 5.45 \times B + 2.26 \times C + 0.04 \times A \times B + 2.11E-003 \times A \times C - 3.0E-004 \times B \times C - 0.01 \times A^2 - 0.50 \times B^2 - 0.04 \times C^2 \quad (2)$$

where, A: temperature (°C), B: Pressure (MPa), C: holding time (min).

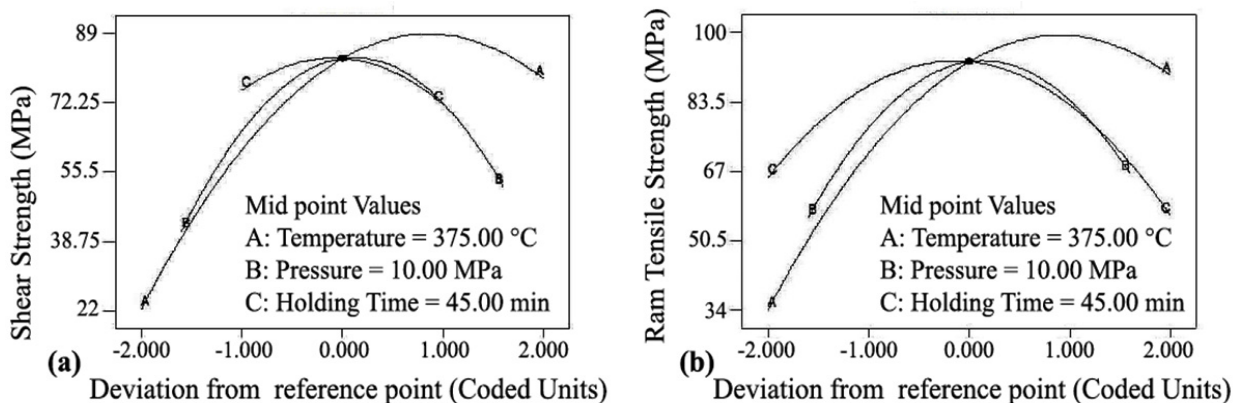


FIGURE 9. Perturbation chart of bonding process: (a) Lap Shear (b) Ram Tensile.

RSM is used to determine the best set of process parameters for obtaining a maximum or minimum answer value (Singh *et al.*, 2017). Via 3D surface plots and contour plots, the optimized input parameters for obtaining the maximum shear and ram tensile strength were realized in this work. Figures 10 and 11 show the 3D surface plots for shear and tensile power, as well as their contour plots. Figure 10a shows that the shear strength increases with increasing temperature and pressure, but these factors become saturated at their mid-range values, and that further increases in these factors are detrimental to the strength. Sound bonding occurs in the temperature range of 382 °C to 410 °C, according to the contour map. Similarly, Fig.10b supports the same temperature range for achieving high shear power, regardless of the keeping period used in the exper-

iment. The effect of pressure and keeping time on shear strength is shown in Fig. 10c. It's designed to keep the pressure between 9 and 15 MPa and the holding time between 45 and 60 min.

The effect of pressure and temperature on the ram tensile strength of the bonded joints is shown in Fig. 11a. The ram tensile strength is also optimum at the mid-range value of the process parameters, similar to the shear strength. The contour plot indicates that the temperature for sound joints should be kept between 370 °C and 410 °C, and the pressure should be kept between 5 MPa and 15 MPa. The holding time should be held between 35 and 50 min, as shown in Fig. 11b, which was further supported by the contour plot in Fig. 11c.

Overlay counterplots were used for graphical optimization to select the best process parameters from

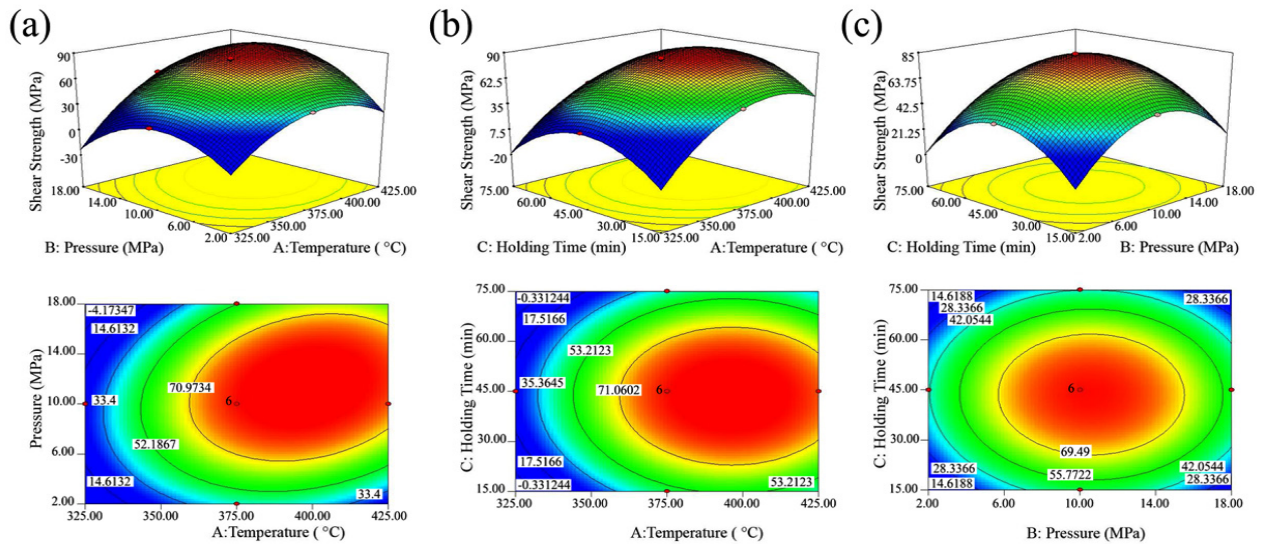


Figure 10. 3D Surface plots for Shear strength along with its contour plot.

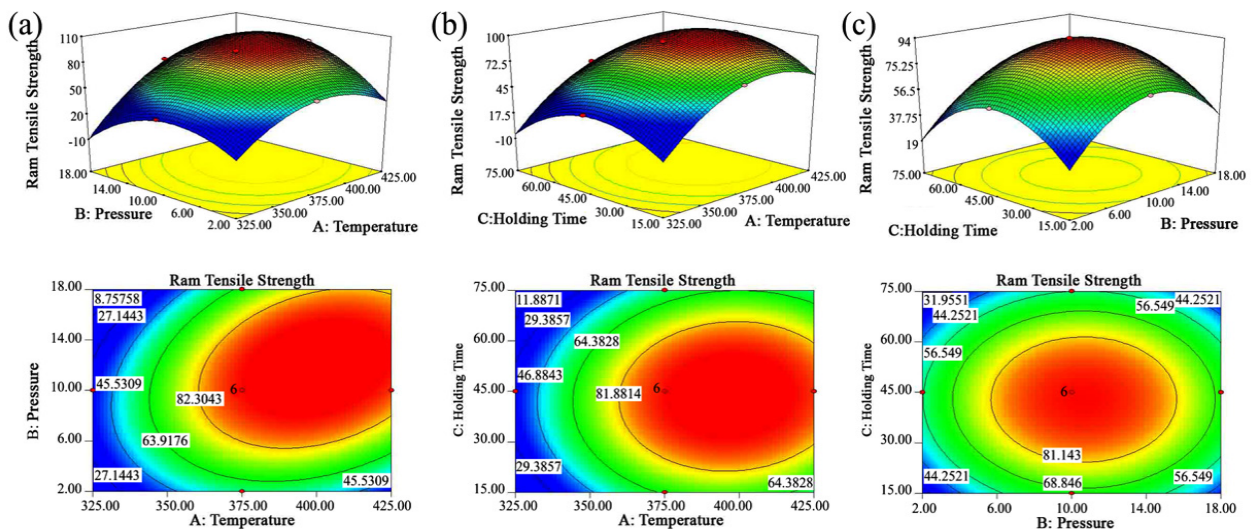
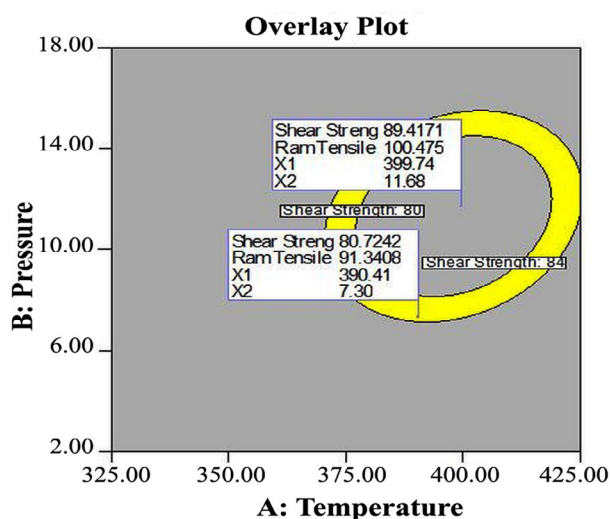


Figure 11. 3D Surface plots for Ram tensile strength along with its contour plot

the planned domain for optimum power (Fig. 12). With respect to temperature and pressure, the overlay plot shows the coordinates for the optimum pressure and temperature conditions at a holding time of 46 min and 43 sec. Experiments were conducted in the expected conditions, and the maximum shear and ram tensile strengths of  $84.1 \pm 0.7$  MPa and  $93.8 \pm 0.6$  MPa respectively, were obtained. The experimental results are similar to the expected values, indicating that the model is accurate.



**Figure 12.** Overlay graphical plot representation of optimal process conditions for maximizing the bond strength.

#### 4. CONCLUSIONS

To optimize the lap shear and ram tensile strength of AA 2014 / AA7075 Al alloys, diffusion bonds were made under various influencing process conditions. The following are the key conclusions drawn from this study:

- Empirical relationships were established between process parameters and diffusion bond shear and ram tensile strength between AA2014 and AA7075 Al alloys to accurately predict diffusion bond strength at a 95% confidence level.
- Atomic diffusion and the formation of inter-diffusional elements phases are confirmed by elemental mapping. The micrograph shows how the thickness of the interface layer varies depending on the process conditions.
- The diffusion bond's strength increases with interface thickness until it reaches  $6 \mu\text{m}$ , after which it deteriorates. For higher bond strength joints, the microhardness plot across the bond surface shows a bell-shaped curve, indicating that the formation of inter-diffusional elements phases occurs in a narrow bandwidth.
- For optimum shear strength and ram tensile strength, the bonding temperature should be

between  $370$  and  $410$  °C, the pressure should be between  $9$  and  $15$  MPa, and the holding time should be between  $35$  and  $50$  min.

#### ACKNOWLEDGEMENT

The authors express their heartfelt gratitude to the Department of Science and Technology (DST), New Delhi, for providing financial assistance through the INSPIRE Fellowship to pursue his PhD studies.

The authors are grateful to V. Balasubramanian, Professor, Center for Materials Joining and Study (CEMAJOR), Department of Manufacturing Engineering, Annamalai University, Annamalai Nagar, India, for allowing them to conduct this research using metal joining and material testing facilities.

#### REFERENCES

- Britto, A.S.F., Raj, R.E., Mabel, C.M. (2017). Prediction of shear and tensile strength of the diffusion bonded AA5083 and AA7075 aluminium alloy using ANN. *Mater. Sci. Eng. A* 692, 1-8. <https://doi.org/10.1016/j.msea.2017.03.056>.
- Britto, A.S.F., Raj, R.E., Mabel, C.M. (2018). Prediction and optimization of mechanical strength of diffusion bonds using integrated ANN-GA approach with process variables and metallographic characteristics. *J. Manuf. Process.* 32, 828-838. <https://doi.org/10.1016/j.jmapro.2018.04.015>.
- Britto, A.S.F., Raj, R.E., Mabel, C.M. (2020). Design of bonding process parameters for experimentation and ANN-GA model development to maximize diffusion bond strength. *Int. J. Comput. Mater. Sci. Surf. Eng.* 9 (3), 177-197. <https://doi.org/10.1504/IJCMSSE.2020.10032744>.
- Britto, A.S.F., Binoj, J.S., Manikandan, N., Surendranatha, G.M., Naidu, B.V.V., Saji Raveendran, P. (2022). Effect of interfacial thickness on microstructure, mechanical properties, and modelling of diffusion fused dissimilar Al alloys for process optimization using ANN-GA method. *Multiscale and Multidiscip. Model. Exp. and Des.* 5, 105-117. <https://doi.org/10.1007/s41939-021-00106-5>.
- Cai, D., Han, S., Zheng, S., Luo, Z., Zhang, Y., Wang, K. (2018). Microstructure and corrosion resistance of Al5083 alloy hybrid plasma-MIG welds. *Journal of Materials Processing Technology* 255, 530-535. <https://doi.org/10.1016/j.jmapro.2017.12.033>.
- Campbell, F.C. (2006). *Manufacturing technology for aerospace structural materials*. Butterworth-Heinemann Publication, New York, USA.
- Fernandus, M.J., Senthilkumar, T., Balasubramanian, V., Rajakumar, S. (2012). Optimising diffusion bonding parameters to maximize the strength of AA6061 aluminium and AZ31B magnesium alloy joints. *Mater. Design* 33, 31-41. <https://doi.org/10.1016/j.matdes.2011.06.022>.
- Grard, C. (1920). *Aluminium and Its Alloys*. Constable & Company Ltd., Warrington, C.Y Kong, R.C Soar.
- He, P., Feng, J.C., Zhang, B.G., Qian, Y.Y. (2002). Microstructure and strength of diffusion bonded joints of Ti Al base alloy to steel. *Mater. Charact.* 48 (5), 401-406. [https://doi.org/10.1016/S1044-5803\(02\)00319-4](https://doi.org/10.1016/S1044-5803(02)00319-4).
- Hill, A., Wallach, E.R. (1989). Modelling Solid-State Diffusion Bonding. *Acta Metall.* 37 (9), 2425-2431. [https://doi.org/10.1016/0001-6160\(89\)90040-0](https://doi.org/10.1016/0001-6160(89)90040-0).
- Huang, Y., Ridley, N., Humphreys, F.J., Cui, J.Z. (1999). Diffusion bonding of superplastic 7075 aluminium alloy. *Materials Science and Engineering A* 266 (1-2), 295-302. [https://doi.org/10.1016/S0921-5093\(98\)00958-7](https://doi.org/10.1016/S0921-5093(98)00958-7).
- Huang, L., Wu, D., Hua, X., Liu, S., Jiang, Z., Li, F., Wang, H., Shi, S. (2018). Effect of the welding direction on the microstructural characterization in fiber laser-GMAW hy-

- brid welding of 5083 aluminum alloy. *J. Manuf. Process.* 31, 514-522. <https://doi.org/10.1016/j.jmapro.2017.12.010>.
- Huiping, L., Guoqun, Z., Shanting, N., Yiguo, L. (2007). Technologic parameter optimization of gas quenching process using response surface methods. *Comput. Mater. Sci.* 38 (4), 561-70. <https://doi.org/10.1016/j.commatsci.2006.03.014>.
- Ilangovan, M., Rajendra Boopathy, S., Balasubramanian, V. (2015). Microstructure and tensile properties of friction stir welded dissimilar AA6061/AA5086 aluminium alloy joints. *Trans. Nonferrous Met. Soc. China* 25 (4), 1080-1090. [https://doi.org/10.1016/S1003-6326\(15\)63701-3](https://doi.org/10.1016/S1003-6326(15)63701-3).
- Kazakov, N.F. (1985). *Diffusion Bonding of Materials*. Mir Publishers, Moscow.
- Kong, C.Y., Soar, R.C., Dickens, P.M. (2004). Optimum process parameters for ultrasonic consolidation of 3003 aluminium. *J. Mater. Process. Technol.* 146 (2), 181-187. <https://doi.org/10.1016/j.jmatprotec.2003.10.016>.
- Li, H., Zou, J., Yao, J., Peng, H. (2017). The effect of TIG welding techniques on microstructure, properties and porosity of the welded Joint of 2219 aluminum alloy. *J. Alloys Compd.* 725, 531-539. <https://doi.org/10.1016/j.jallcom.2017.08.157>.
- Mahendran, G., Balasubramanian, V., Senthilvelan, T. (2009). Developing diffusion bonding windows for joining AZ31B magnesium-AA 2024 Aluminium alloys. *Mater. Design* 30 (4), 1240-1244. <https://doi.org/10.1016/j.matdes.2008.06.015>.
- Morley, R.A., Caruso, J. (1980). Diffusion welding of 390 aluminium alloy hydraulic valve bodies. *Welding Journal*, 29-34.
- Palanisamy, D., Britto, A.S.F., Binoj, J.S., Manikandan, N. (2021). Statistical Optimization of Parameters for Enhanced Properties of Diffusion Bonded AA6061 and AA 7075 Aluminium Alloys. *Mater. Today: Proc.* 39 (Part 1), 388-397. <https://doi.org/10.1016/j.matpr.2020.07.614>.
- Peterson, K.A., Dutta, I., Chen, M. (2004). Processing and characterization of diffusion-bonded Al-Si interfaces. *J. Mater. Process. Technol.* 145 (1), 99-108. [https://doi.org/10.1016/S0924-0136\(03\)00877-X](https://doi.org/10.1016/S0924-0136(03)00877-X).
- Pilling, J., Ridley, N. (1987). Solid state bonding of superplastic AA 7475. *Mater. Sci. Technol.* 3 (5), 353-359. <https://doi.org/10.1179/mst.1987.3.5.353>.
- Kadaganchi, R., Gankidi, M.R., Gokhale, H. (2015). Optimization of process parameters of aluminum alloy AA 2014-T6 friction stir welds by response surface methodology. *Def. Technol.* 11 (3), 209-219. <https://doi.org/10.1016/j.dt.2015.03.003>.
- Singh, A., Garg, H., Lall, A.K. (2017). Optical polishing process: Analysis and optimization using response surface methodology (RSM) for large diameter fused silica flat substrates. *J. Manuf. Process.* 30, 439-451. <https://doi.org/10.1016/j.jmapro.2017.10.017>.
- Sunwoo, A.J. (1993). *Diffusion Bonding of Superplastic Aluminum Alloys*. National Technical Information Service U.S. Department of Commerce, pp. 1-8.
- Sunwoo, A., Lum, R. (1995). Superplastic Deformation Enhanced Diffusion Bonding of Aluminum Alloy 7475. *Scripta Metall. Mater.* 33 (4), 639-644. [https://doi.org/10.1016/0956-716X\(95\)00224-J](https://doi.org/10.1016/0956-716X(95)00224-J).
- Velmanirajan, K., Abu Thaheer, A.S., Narayanasamy, R., Ahamed Basha, C. (2012). Numerical modelling of aluminum sheets formability using response surface methodology. *Materials and Design* 41, 239-254. <https://doi.org/10.1016/j.matdes.2012.05.027>.
- Wang, Y., Luo, G., Zhang, J., Shen, Q., Zhang, L. (2012). Effect of silver interlayer on microstructure and mechanical properties of diffusion-bonded Mg-Al joints. *J. Alloys Compd.* 541, 458-461. <https://doi.org/10.1016/j.jallcom.2012.06.120>.
- Wang, L., Wei, Y., Zhao, W., Zhan, X., She, L. (2018). Effects of welding parameters on microstructures and mechanical properties of disk laser beam welded 2A14-T6 aluminum alloy joint. *J. Manuf. Process.* 31, 240-246. <https://doi.org/10.1016/j.jmapro.2017.11.017>.
- Wu, Y.E., Lo, Y.L. (2002). Surface protection for AA8090 aluminum alloy by diffusion bonding. *Theor. Appl. Fract. Mech.* 38 (1), 71-79. [https://doi.org/10.1016/S0167-8442\(02\)00082-4](https://doi.org/10.1016/S0167-8442(02)00082-4).
- Zhao, L.M., Zhang, Z.D. (2008). Effect of Zn alloy interlayer on interface microstructure and strength of diffusion-bonded Mg-Al joints. *Scripta Mater.* 58 (4), 283-286. <https://doi.org/10.1016/j.scriptamat.2007.10.006>.